Hindawi Publishing Corporation
International Journal of Photoenergy
Volume 2013, Article ID 452542, 10 pages
http://dx.doi.org/10.1155/2013/452542

Research Article

Dynamic Hydrogen Production from Methanol/Water Photo-Splitting Using Core@Shell-Structured CuS@TiO_2 Catalyst Wrapped by High Concentrated TiO_2 Particles

Younghwan Im,[1] Sora Kang,[1] Kang Min Kim,[1] Taeil Ju,[1] Gi Bo Han,[2] No-Kuk Park,[3] Tae Jin Lee,[3] and Misook Kang[1]

[1] *Department of Chemistry, College of Science, Yeungnam University, Gyeongsan, Gyeongbuk 712-749, Republic of Korea*
[2] *Plant Engineering Division, Institute for Advanced Engineering, 633-2 Goan-ri, Baegam-myeon, Cheoin-gu, Yongin-si, Gyeonggi 449-863, Republic of Korea*
[3] *School of Chemical Engineering, Yeungnam University, Gyeongsan, Gyeongbuk 712-749, Republic of Korea*

Correspondence should be addressed to Misook Kang; mskang@ynu.ac.kr

Received 12 July 2013; Revised 1 August 2013; Accepted 1 August 2013

Academic Editor: Jiaguo Yu

This study focused on the dynamic hydrogen production ability of a core@shell-structured CuS@TiO_2 photocatalyst coated with a high concentration of TiO_2 particles. The rectangular-shaped CuS particles, 100 nm in length and 60 nm in width, were surrounded by a high concentration of anatase TiO_2 particles (>4~5 mol). The synthesized core@shell-structured CuS@TiO_2 particles absorbed a long wavelength (a short band gap) above 700 nm compared to that pure TiO_2, which at approximately 300 nm, leading to easier electronic transitions, even at low energy. Hydrogen evolution from methanol/water photo-splitting over the core@shell-structured CuS@TiO_2 photocatalyst increased approximately 10-fold compared to that over pure CuS. In particular, 1.9 mmol of hydrogen gas was produced after 10 hours when 0.5 g of 1CuS@4TiO_2 was used at pH = 7. This level of production was increased to more than 4-fold at higher pH. Cyclic voltammetry and UV-visible absorption spectroscopy confirmed that the CuS in CuS@TiO_2 strongly withdraws the excited electrons from the valence band in TiO_2 because of the higher reduction potential than TiO_2, resulting in a slower recombination rate between the electrons and holes and higher photoactivity.

1. Introduction

In recent years, hydrogen has been highlighted as a next-generation energy source because of its environmentally friendly nature and high-energy efficiency. Therefore, hydrogen production has recently become the most active research topic globally. In particular, the technology for generating hydrogen by the splitting of water using a photocatalyst has attracted considerable attention. In the early days, the photocatalytic formation of hydrogen and oxygen focused extensively on metal-loaded or incorporated-TiO_2 semiconductors due to the low band gap and high corrosion resistance of these materials [1–5]. On the other hand, hydrogen production from water photo-splitting using TiO_2-based photocatalysts is ineffective because the amount of hydrogen produced is limited by the rapid recombination of holes and electrons over TiO_2, resulting in the reformation of water [6]. In addition, more than 1.2 eV is needed to decompose water [7], which means that the photodecomposition of water should be performed at UV wavelengths of approximately 260 nm. Therefore, there is urgent need for the development of new and inexpensive photocatalysts that are both environmentally friendly and possess greater hydrogen-producing activity under visible light irradiation. Recently, studies of metal sulfide photocatalysts, such as ZnS- [8], CuS- [9, 10], FeS- [11], Bi_2S_3- [12], Sb_2S_3- [13], or CdS-loaded TiO_2 [14], have covered topics ranging from synthesis to applications in new photocatalytic reaction mechanisms. Narrow band gaps make it possible to absorb longer wavelengths compared to wide band gaps of conventional metal oxide semiconductor systems. A previous study reported high photocatalytic activity on the ZnS-loaded TiO_2 composite system for hydrogen

production [15]. In that study, the evolution of H_2 from methanol/water (1 : 1) photo-splitting over the ZnS/TiO_2 composite was enhanced dramatically compared to that over pure TiO_2 and ZnS. In particular, 1.2 mmol of H_2 gas was produced after 10 h when 0.5 g of a 5.0 wt% ZnS-loaded TiO_2 composite was used. Recently, many studies began to focus their attention on bimetallic sulfides photocatalysts, such as CdZnS [16], CuZnS [17], ZnInS [18], and AgZnS [19]. These studies have been extended to trimetallic sulfide photocatalysts, such as CuAgInS [20], ZnCuCdS [21], CuInZnS [22], and AgGaInS [23]. On the other hand, most papers are based on metal sulfides loaded on the surface of TiO_2 particles. Few studies have examined TiO_2 nanoparticles loaded on the surface of large-sized metal sulfide particles.

This study focused on the CuS core material with a shorter band-gap of 1.56 eV and a higher reduction potential [24] than those of pure TiO_2. Cu materials are widely used as catalysts for methanol steam reforming because of their excellent redox properties despite vulnerable to water. The potential ($Cu^{2+} + 2e^- = Cu^0$, $E^\circ = -0.224$ V) is slightly lower than the conduction band (−0.26 V) of anatase TiO_2 but is higher than the reduction potential of H^+ ($2H^+ + 2e^- = H_2$, $E^\circ = -0.000$ V), which favors electron transfer from the conduction band of TiO_2 to Cu^{2+}, and the reduction of H^+, thereby enhancing the photocatalytic H_2-production activity [25, 26]. In this study, CuS was synthesized by a hydrothermal method with sodium sulfate as the sulfur source. A Ti precursor at a high concentrated molar ratio was then coated on the surface of the CuS like a core-shell structure. The relationship between the spectroscopic properties and the catalytic performance for the hydrogen production over the core@shell-structured $CuS@TiO_2$ was examined by X-ray diffraction (XRD), transmission electron microscopy (TEM), UV-visible absorption spectroscopy, Brunauer, Emmett, and Teller (BET) surface areas, cyclic voltammetry (CV), and zeta potential measurements using an electrophoresis measurement apparatus.

2. Experimental

2.1. Synthesis of CuS and Core@Shell-Structured $CuS@TiO_2$. The TiO_2, CuS, and core@shell-structured $CuS@TiO_2$ photocatalysts were prepared using hydrothermal and impregnation methods, respectively. In the first step for TiO_2, titanium tetra-isopropoxide (TTIP, 99.99%, Junsei Chemical, Japan) as a titanium precursor was added dropwise to an aqueous solution and stirred homogeneously for 2 h. The pH of the final solution was set to pH = 3.0 using acetic acid to induce mild hydrolysis, and the resulting solution was transferred to an autoclave for thermal treatment. The thermal treatment at 200°C was kept for 12 h, and the resulting precipitates were obtained, washed with distilled water, and dried at 80°C for 24 h. In the second step of CuS synthesis, $CuSO_4 \cdot 5H_2O$ (99.99%, Junsei Chemical, Japan) and $Na_2S_2O_3 \cdot 5H_2O$ (99.99%, Junsei Chemical, Japan) were used as the Cu and S precursors to prepare the sol mixture, respectively. Copper sulfate and sodium sulfate were dissolved sequentially in distilled water and stirred to homogeneity for 2 h. The final solution was transferred to an autoclave for thermal treatment. Cu ions were sulfurized during the thermal treatment at 180°C for 12 h. The resulting precipitates were obtained, washed with distilled water, and dried at 80°C for 24 h. Finally the dried powders were treated at 400°C for 4 h to obtain crystallized CuS. Finally, 4.0 and 5.0 moles of TTIP (titanium tetraisopropoxide, 99.99%, Aldrich) for each 1.0 mole of CuS were added slowly to an ethanol solution containing the dispersed CuS particles during stirring to coat the CuS surface. The pH of the colloidal solution was kept at 4.0, and the solution was stirred homogeneously for 18 h. The final solution was evaporated at 80°C for 5 h and calcined at 400°C for 4 h to induce the anatase TiO_2. Finally, three types of materials, CuS and the core@shell-structured $1CuS@4TiO_2$ and $1CuS@5TiO_2$, were examined. Three samples of pure TiO_2 (by hydrothermal method), CuS, and physically mixed TiO_2/CuS were also prepared for comparison.

2.2. Characteristics of Synthesized CuS and Core@Shell-Structured $CuS@TiO_2$. The synthesized CuS and core@shell-structured $CuS@TiO_2$ photocatalysts were examined by XRD (X'Pert Pro *MPD PANalytical* 2-circle diffractometer) using nickel-filtered CuKα radiation (30 kV and 30 mA). The sizes and shapes of the CuS and core@shell-structured $CuS@TiO_2$ photocatalysts were examined by TEM (JEOL 2000EX). The BET surface areas of catalysts were measured using a Belsorp II instrument. All the catalysts were degassed under vacuum at 150°C for 30 min before the BET surface measurements. The catalysts were measured through the nitrogen gas adsorption using a continuous flow method with a mixture of nitrogen and helium as the carrier gas. The UV-visible absorption spectra of CuS and core@shell-structured $CuS@TiO_2$ powders were obtained using a Cary 500 spectrometer with a reflectance sphere. The CV measurements of the CuS and core@shell-structured $CuS@TiO_2$ pellets were obtained using a BAS 100B potentiostat at room temperature in 0.1 M KCl solution. A platinum wire as the counter electrode and Ag/AgCl as the reference electrode were used. The zeta potential of CuS and core@shell-structured $CuS@TiO_2$ particles was determined by the electrophoretic mobility using an electrophoresis measurement apparatus (ELS 8000, Otsuka Electronics, Japan) with a plate sample cell. Electrophoretic light scattering (ELS) was performed in reference beam mode using a laser light source of 670 nm, a modular frequency of 250 Hz, and a scattering angle of 15°. The standard error of the zeta potential, converted from the experimentally determined electrophoretic mobility, was typically <1.5%, and the percentage error was <5%. To measure the zeta potentials, 0.1 wt% of each sample was dispersed in deionized water, and the pH of the solution was adjusted with HCl or NaOH. The relative molecular diameter size distributions of the various solutions were also measured using this equipment.

2.3. Hydrogen Production from Photo-Splitting of Methanol/Water over CuS and Core@Shell-Structured $CuS@TiO_2$. Photo-splitting in methanol/water using CuS and core@shell-structured $CuS@TiO_2$ photocatalysts was carried out using a liquid photoreactor designed in house, as shown in Figure 1.

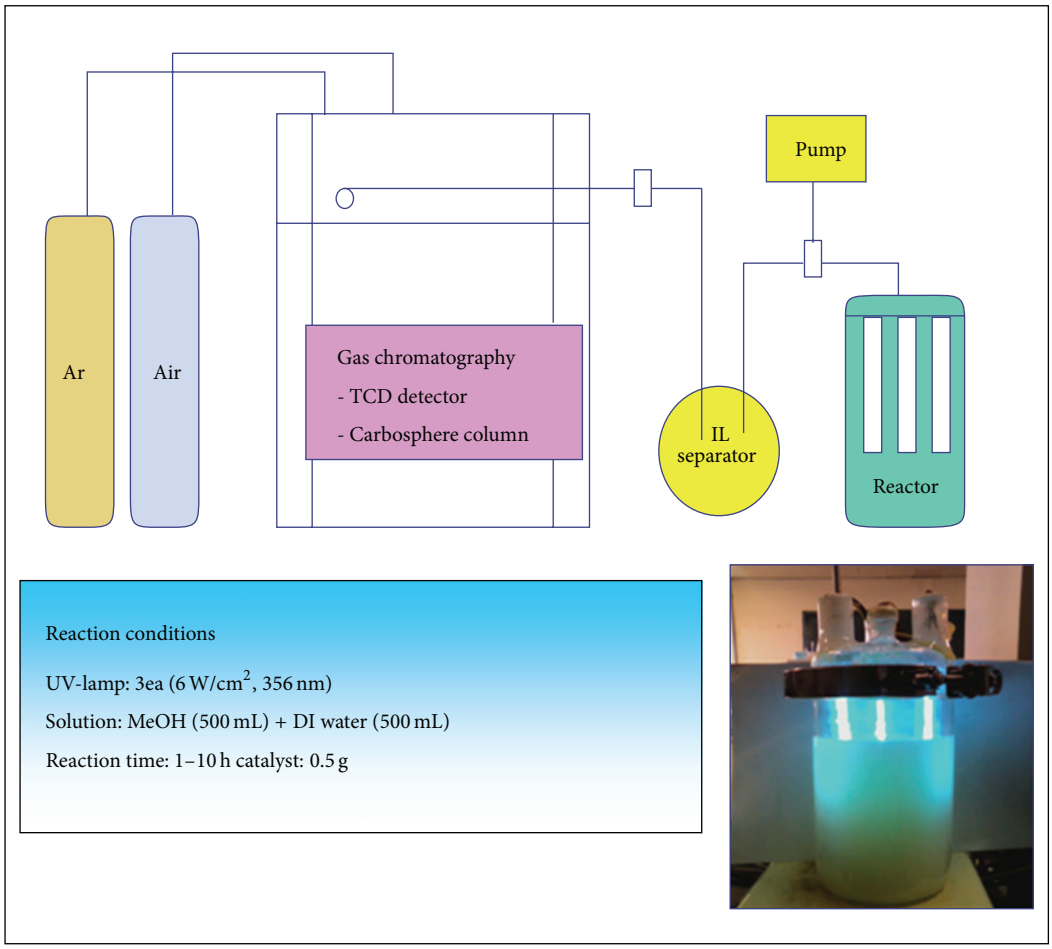

Figure 1: Apparatus of a liquid photoreactor for the methanol/water photo-splitting using CuS and core@shell-structured CuS@TiO_2 photocatalysts.

For methanol/water photo-splitting, 0.5 g of a photocatalyst was added to 1.0 L distilled water in a 2.0 L Pyrex reactor. UV-lamps (6×3 W cm^{-2} = 18 W cm^{-2}, 30 cm length × 2.0 cm diameter; Shinan Co.) emitting radiation with a wavelength of 365 nm were used. Methanol/water photo-splitting was carried out for 10 h with constant stirring, and the level of hydrogen evolution was measured at 1 h intervals. The hydrogen gas (H_2) produced during methanol/water photo-splitting was analyzed by TCD-type gas chromatography (GC, model DS 6200; Donam Instruments Inc., Republic of Korea). To determine the products and intermediates, the GC was connected directly to the methanol/water photo-splitting reactor. The following GC conditions were used: TCD detector; Carbosphere column (Alltech, Deerfield, IL, USA); and an injection, initial, final, and detector temperature of 413 K, 393 K, 393 K, and 423 K, respectively.

3. Results and Discussion

3.1. Properties of Synthesized CuS and Core@Shell-Structured CuS@TiO_2. Figure 2 shows XRD patterns of the TiO_2, CuS,

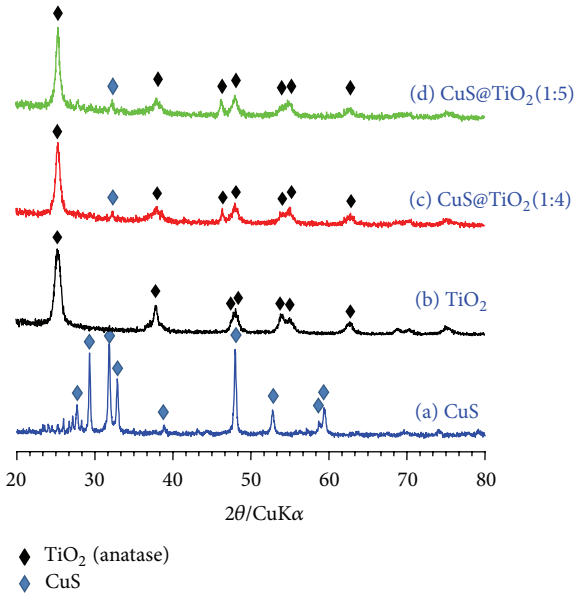

Figure 2: XRD patterns of the CuS and CuS@TiO_2 photocatalysts.

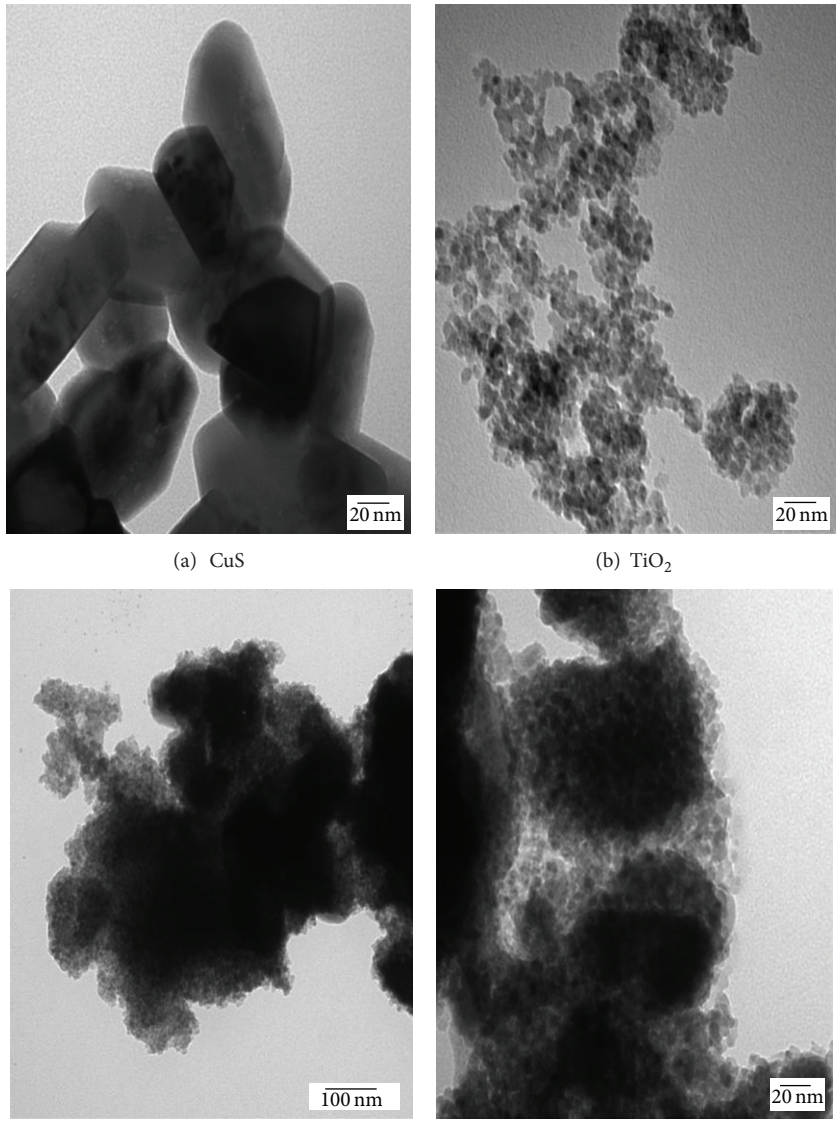

(a) CuS (b) TiO_2

(c) CuS@TiO_2 (1 : 4) (d) CuS@TiO_2 (1 : 5)

Figure 3: TEM images of the CuS and CuS@TiO_2 photocatalysts.

and CuS@TiO_2 photocatalysts. All the peaks in CuS were indexed to the hexagonal phase CuS (P63/mmc space, cell constants $a = 3.8$ Å, $b = 3.8$ Å, and $c = 16.43$ Å; JCPDS Card no. 02-0820). The XRD patterns showed the main peaks at 26.75, 27.51, 29.36, 31.82, 33.03, 38.96, 43.04, 44.60, 52.88, 59.18, 63.69, 67.86, 69.58, 74.00, and 79.08° 2θ, which were assigned to the (100), (101), (102), (103), (006), (105), (106), (008), (110), (114), (116), (1010), (0012), (207), (208), and (213) planes, respectively. In the case of CuS@TiO_2, the peaks for crystalline CuS almost disappeared except for a very small peak at 33.03° 2θ (006). This result coincides with the fact that in general if the core-shell structure formed completely in a core-shell material, the XRD peaks for the core do not appear; only the diffraction patterns for the shell are observed [27]. Otherwise, the XRD patterns for crystalline TiO_2 (anatase, tetragonal crystal system, I41/amd space, JCPDS Card no. 02-0387) in CuS@TiO_2 were observed at 25.35, 37.93, 48.10, 53.89, 55.30, 68.99, 70.18, and 75.37° 2θ, which were assigned to the (101), (004), (200), (105), (211), (116), (220), and (215) planes, respectively. The locations were the same as the hydrothermally prepared pure TiO_2 in (b). The peaks in CuS@TiO_2 were slightly larger according to the loaded Ti concentration. The XRD peak intensities that were assigned to anatase TiO_2 in 1CuS@5TiO_2 were slightly sharper than those of CuS@TiO_2 loaded with 4.0 mol-concentrated Ti. Generally, the line widths of the XRD peaks were broad, which indicated a smaller crystallite size. The Scherrer equation, $t = 0.9\lambda/\beta\cos\theta$, where λ is the wavelength of incident X-rays, β is the full width at half maximum (FWHM) in radians, and θ is the diffraction angle,

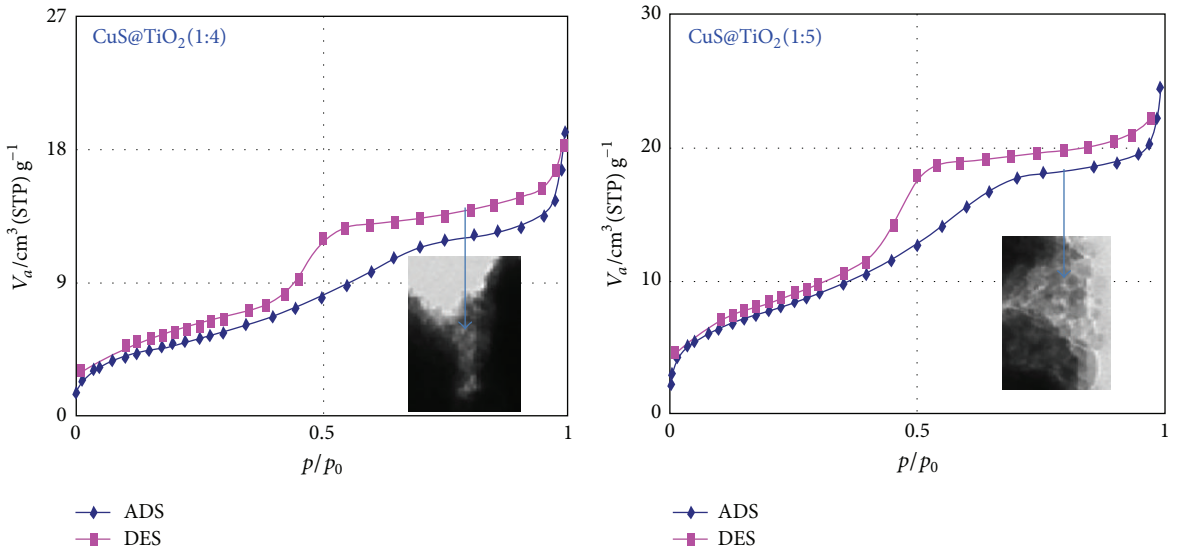

(a) (b)

	CuS@TiO_2(1:4)	CuS@TiO_2(1:5)
Surface area ($m^2\ g^{-1}$)	17.88	27.966
Total pore volume ($cm^3\ g^{-1}$)	0.02973	0.037988
Average pore diameter (nm)	6.651	5.4334

(c)

Figure 4: Adsorption-desorption isotherm curves of N_2 at 77 K for the core@shell-structured CuS@TiO_2.

was used to determine the crystallite size. The loaded TiO_2 crystallite sizes of 1CuS@4TiO_2 and 1CuS@5TiO_2 based on the 25.35° 2θ peak were 17.50 and 17.90 nm, respectively.

Figure 3 shows TEM images of the CuS and CuS@TiO_2 powders. Rectangular-shaped particles with 100 nm long and 60 nm wide sides were observed in the CuS sample, and 10 nm sized TiO_2 particles were also observed in TiO_2 samples. Here, the nanosized TiO_2 particles were synthesized hydrothermally for comparison. Interestingly, the huge CuS particles were surrounded by nanosized TiO_2 particles with high concentrations (4~5 moles compared to 1 mole of core CuS). This is in good agreement with the XRD patterns. This is a reliable result in that, when the loaded TiO_2 amounts increased, the shell composed of TiO_2 particles was thicker. TEM confirmed that the obtained CuS@TiO_2 sample had a core@shell structure.

Figure 4 shows the adsorption-desorption isotherm curves of N_2 at 77 K for the fresh powder samples and core@shell-structured CuS@TiO_2. The isotherms belonged to the IV type in the IUPAC classification [28]. Generally, this hysteresis slope has been observed in the presence of large mesopores. Here, the mesopores are considered to be bulk pores formed between TiO_2 particles in the shell. This suggests that the reaction of the catalyst with a high surface area facilitates adsorption, which can improve the catalytic activity. Therefore, it is expected that the methanol or water molecules are adsorbed more easily on the surfaces of the core@shell-structured CuS@TiO_2 than those of pure TiO_2 or CuS particles during methanol/water photo-splitting. The surface area increased from 17.88 to 27.97 $m^2\ g^{-1}$ according to the change in TiO_2 concentration from 4.0 to 5.0 mol. Generally, the specific surface area increases with decreasing particle size. Here, the loaded TiO_2 particle sizes in the two samples were similar. Therefore, the surface area in this study possibly depends on the bulk pores formed by aggregation between the TiO_2 particles in the shell. The total bulk-pore volumes increased from 0.029 (4 mol TiO_2 loading) to 0.038 (5 mol TiO_2 loading) $cm^3\ g^{-1}$. Eventually, the specific surface area increased with increasing pore volume.

Figure 5 shows the UV-visible absorption spectra of the CuS and core@shell-structured CuS@TiO_2 powders. The absorption edges of Ti^{4+} and Cu^{2+} with octahedral symmetries normally appear at a maximum of approximately 300 and 700 nm in pure TiO_2 and CuS, respectively [29, 30]. The band gap in a semiconductor material is closely related to the wavelength range absorbed, where the band gap decreases with increasing absorption wavelength. Consequently, a material with a narrow band gap can be extended readily to utilize visible light, whereas a narrow band gap can reduce photocatalytic activity by increasing the recombination rate

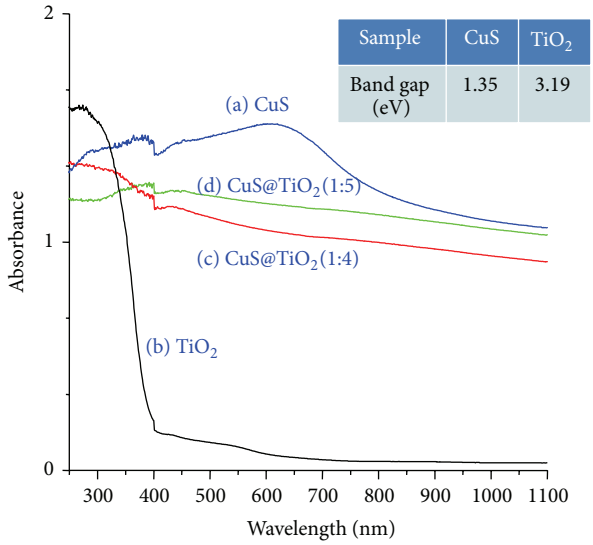

FIGURE 5: UV-visible absorption spectra of the CuS and core@shell-structured CuS@TiO_2 powders.

between the electrons and holes. Based on the Tauc equation [31], the band gaps obtained by extrapolation at the cross-section point of the two tangents were approximately 1.35 and 3.19 eV for pure CuS and TiO_2, respectively.

Figure 6 presents the CV measurements of CuS and the core@shell-structured CuS@TiO_2, indicating high dependence on the analytic conditions being studied, which must be redox active within the experimental potential window. A reversible wave that provides the following information is desirable: reversible reactions will show a ratio of the peak currents passed at reduction (E_{pc}) and oxidation (E_{pa}). When such reversible peaks are observed, thermodynamic information in the form of a half cell potential $E^{\circ}_{1/2}(E_{pc} + E_{pa}/2)$ can be determined. In particular, when the waves are semireversible, such as when $E_{pa}/E_{pc} \geq 1$, it can be possible to induce even more information, particularly in kinetic processes. Recently, some studies reported a useful equation that can determine the energy levels of the HOMO and LUMO using a CV method [32]. In the synthesized CuS, the Cu(II) $\rightarrow$ Cu(0) redox process appeared to be a reversible reaction, and the absolute potential in the reduction (E_{pc}) was observed at −0.732 V. The onset potentials in the core@shell-structured CuS@TiO_2 samples might be used to determine the thermodynamic $E^{\circ}_{1/2}$ as −1.255 and −2.59 V in 1CuS@4TiO_2 and 1CuS@5TiO_2, respectively. The CV curves were observed at two locations, and there might be two factors from TiO_2 (front) and CuS (back), −1.79 and −0.712 V, respectively. Therefore, the corresponding LUMO energy levels were calculated to be −3.65 (for CuS), −3.12 (for 1CuS@4TiO_2), and −3.668 (for 1CuS@5TiO_2) eV, respectively.

Figure 7 summarizes the hydrogen evolution from methanol/water photo-splitting over the CuS, TiO_2, and two types of core@shell-structured CuS@TiO_2 photocatalysts in a batch-type liquid photosystem, and the catalytic performance of a physically mixed CuS+TiO_2 sample was also evaluated for comparison. The catalytic activities of the core@shell-structured CuS@TiO_2 photocatalysts were enhanced considerably compared to the pure CuS or TiO_2. In Figure 7(a), a very small amount of hydrogen was collected over CuS (0.2 mmol) and TiO_2 (0.09 mmol) after methanol/water photo-splitting for 10 h. A significant amount of hydrogen gas was collected over CuS@TiO_2, and the amount of hydrogen produced reached 1.9 mmol over 0.5 g 1CuS@4TiO_2. On the other hand, the amount produced was significantly lower on the core@shell-structured 1CuS@5TiO_2 catalyst with higher Ti incorporation. Here, CuS absorbs longer wavelengths easily, but recombination between the excited electrons and the holes also causes rapid catalytic deactivation. In contrast, the core@shell-structured CuS@TiO_2 has stronger oxidation-reduction ability than pure CuS. Here, the CuS core acts as a good electron collector excited from TiO_2 and transporter, resulting in the retardation of electron-hole recombination, leading to an increase in photocatalytic performance. On the other hand, the collected hydrogen did not increase significantly over the physically mixed CuS+TiO_2 sample. The catalytic performance of methanol/water destruction over the core@shell-structured 1CuS@4TiO_2 was enhanced more under the alkali electrolytes solution, as shown in Figure 7(b). When OH^- ions are present in the alkali solution, the subsequent reaction occurs: OH^- + hole $\rightarrow$ $^{\bullet}OH$ in the valence band. Therefore, a large number of OH radicals are generated in the alkali solution, resulting in an increase in hydrogen evolution. Hydrogen production was increased dramatically in the alkali solution by generating more OH ions, reaching up to 8.0 mmol after 10 h in a KOH (pH = 11) solution. In an acidic solution, however, the level of production was decreased due to SO_4^{2-} ions formed after the reaction. The S ions inside the CuS catalyst appear to dissolve in the acidic solution, followed by a reaction with O ions in water to form SO_4^{2-} ions. Eventually, the sulfate ions combine with the hydrogen ions generated during the methanol/water photo-splitting process, which occurs during the formation of H_2SO_4.

Figure 8 shows the influence of pH on the zeta potential distribution in the CuS, TiO_2, and two types of core@shell-structured CuS@TiO_2. The adjacent table summarizes the aggregated particle sizes in the aqueous solution. The zeta potential of the 1CuS@4TiO_2 suspensions decreased significantly with increasing pH. The surface charges in all samples changed from a positive value in an acidic solution to a larger negative value in an alkali solution. The isoelectric points, meaning the large aggregation of particles, were different: 5.8, 7.9, 7.0, and 7.7 for CuS, TiO_2, 1CuS@4TiO_2, and 1CuS@5TiO_2, respectively. At pH = 11.0, the surface charges in all samples showed the highest absolute value. This suggests that the colloidal samples were stable [33] with high mobility, which is closely related to the reaction sites over the photocatalyst surface. This result matches the results in Figure 6 well.

The CV curves, UV-visible absorption spectra, and their photocatalytic performance suggest a photocatalysis model over the core@shell-structured CuS@TiO_2, as shown in Scheme 1. The TiO_2 shells covered the core CuS completely, which means that the electrons on the valence band of

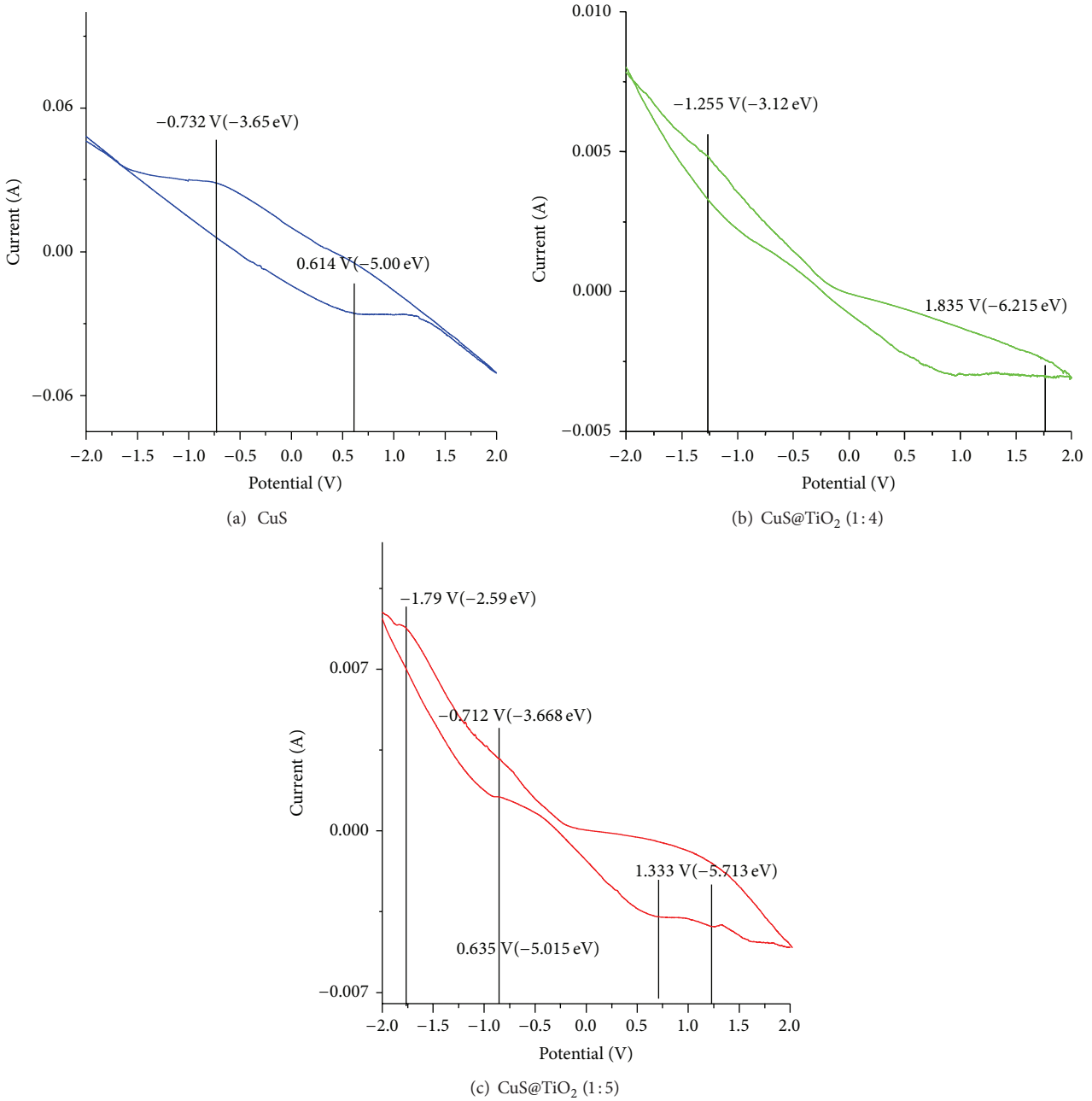

Figure 6: Cyclic voltammetry for the CuS and core@shell-structured CuS@TiO_2.

TiO_2 will be transferred to the conduction band. The excited electrons are moved to the valence band in CuS because of its higher reduction potential than TiO_2. In this study the core CuS acted as a good electron collector and transporter, similar to reduced graphene oxide reported in another paper [34]. Therefore, the recombination of electrons and holes was reduced, and finally more OH radicals were generated easily at the holes in the valence band of TiO_2. Radicals with strong oxidative power attack CH_3OH molecules, and CO_2, H_2, and H_2O are produced by the complete oxidation of methanol. In addition, if the core CuS also absorbs the radiation (if it does not have a complete core@shell structure), the electrons would be excited more easily from the valence band of CuS. Overall, the catalytic activity of CuS@TiO_2 is performed more effectively in the methanol/water photosplitting reaction. This also means that the electrons excited from the valence band over CuS@TiO_2 recombine slowly with the holes during photocatalysis. Therefore, the hole effect at the valence band continues for a longer time than those in pure CuS or TiO_2. In addition, according to the UV-visible spectra, the CuS@TiO_2 samples exhibited enhanced absorbance over the entire visible-light region. Therefore, the CuS core can also absorb visible radiation compared to the TiO_2 shell, which can only absorb UV light. Consequently,

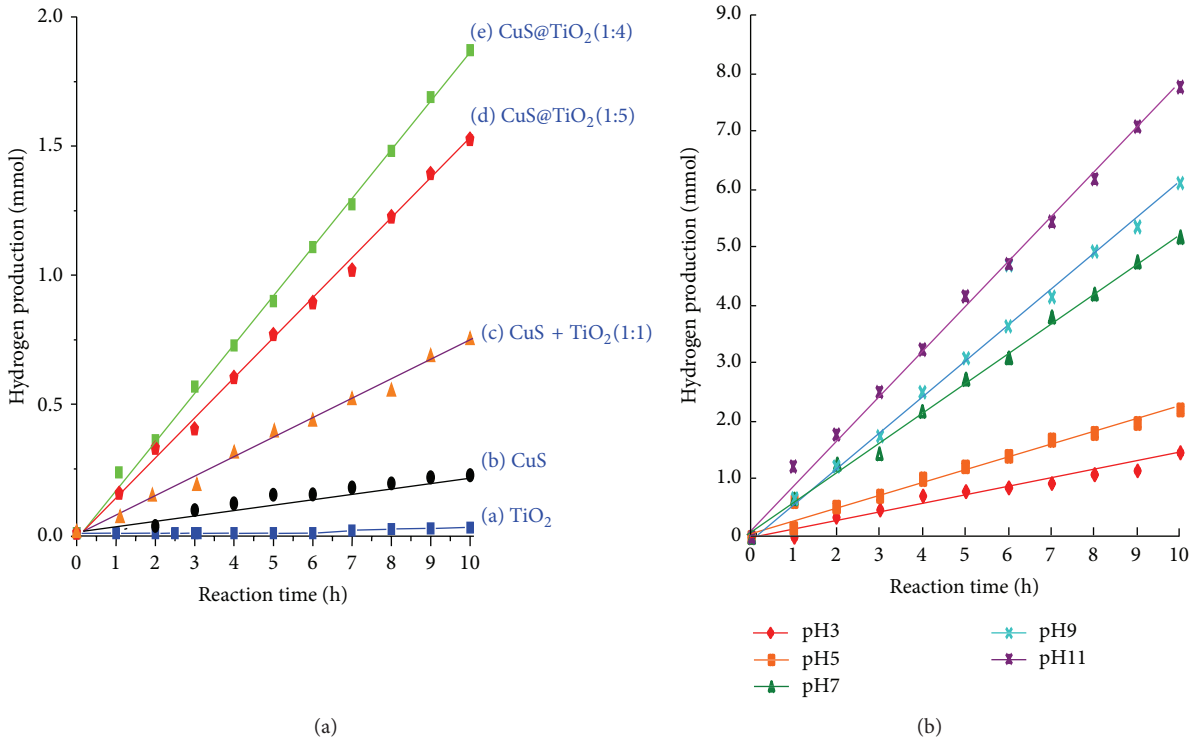

Figure 7: Evolution of H_2 from methanol/water photo-splitting over the CuS, TiO_2, and two types of core@shell-structured CuS@TiO_2 photocatalysts in a batch-type liquid photosystem. (a) Hydrogen production according to the catalysts and (b) hydrogen production according to the pH for 1CuS@4TiO_2.

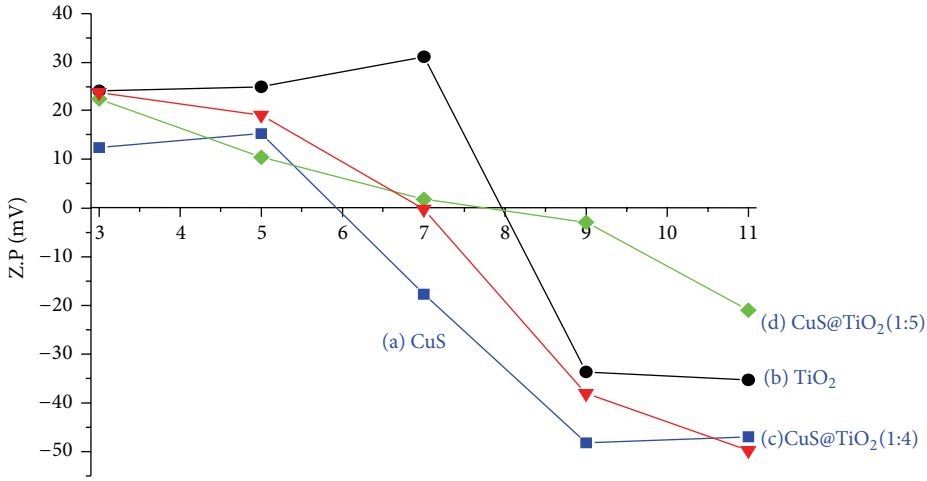

	(a) CuS		(b) TiO_2		(c)CuS@TiO_2(1:4)		(d) CuS@TiO_2(1:5)	
pH	Zeta potential (mV)	Mobility (cm^2/Vs)	Zeta potential (mV)	Mobility (cm^2/Vs)	Zeta potential (mV)	Mobility (cm^2/Vs)	Zeta potential (mV)	Mobility (cm^2/Vs)
3	12.47	9.739e(−4)	24.06	1.944e(−4)	23.76	1.853e(−4)	22.42	1.749e(−4)
5	15.34	1.199e(−5)	24.89	1.944e(−4)	19.13	1.492e(−4)	10.5	8.189e(−5)
7	−17.65	−1.377e(−4)	31.13	4.478e(−4)	−0.23	−1.802e(−6)	1.84	1.435e(−5)
9	−48.24	−3.775e(−4)	−33.61	−2.752e(−4)	−38.08	−2.970e(−4)	−2.88	−2.246e(−4)
11	−47.01	−3.673e(−4)	−35.29	−2.752e(−4)	−49.78	−3.887e(−4)	−20.94	−1.636e(−4)

Figure 8: Zeta potential distributions of the CuS, TiO_2, and two types of core@shell-structured CuS@TiO_2 according to the pH.

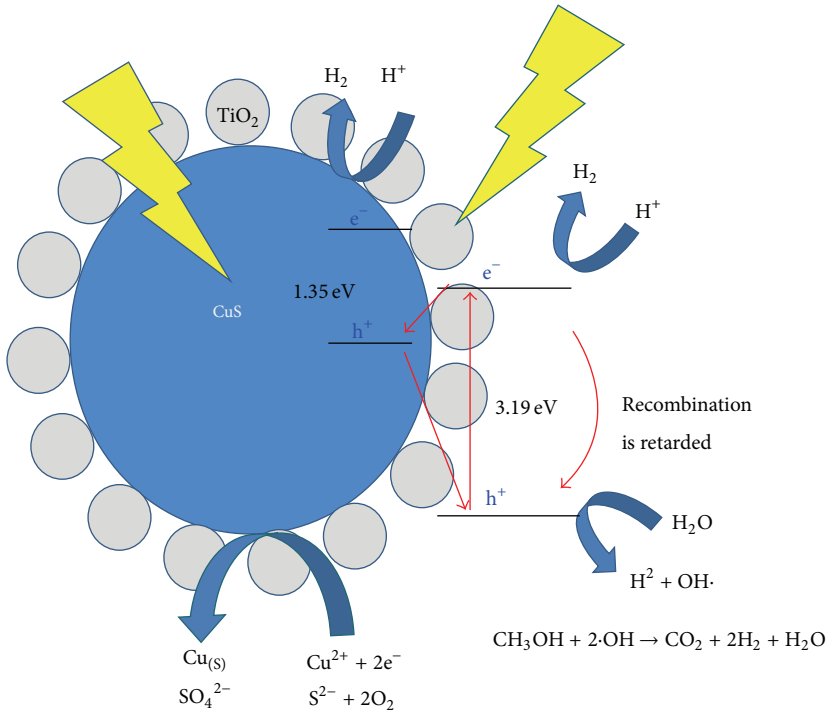

Scheme 1: Supposed photocatalysis model over the core@shell-structured CuS@TiO_2.

the photocatalytic activity is enhanced over the core@shell-structured CuS@TiO_2 photocatalysts.

4. Conclusions

Core@shell-structured CuS@TiO_2 was synthesized using hydrothermal/impregnation methods. Based on the UV-visible absorption and CV results, the band gap of the pure CuS was estimated to be approximately 1.35 eV, respectively, and the corresponding LUMO energy level was −3.65 eV. ELS showed that the core@shell-structured 1CuS@4TiO_2 particles were stable in an alkali solution. A significant amount of hydrogen gas was collected over 0.5 g of the core@shell-structured 1CuS@4TiO_2 photocatalyst, and the amount reached 1.9 mmol with a maximum yield of 8.0 mmol after 10 h in a KOH solution. This was due most likely to the slower recombination between the electrons and a hole, which enables higher catalytic performance over the core@shell-structured 1CuS@4TiO_2. These results are expected to play a significant role in the development of new photocatalysts with a core@shell structure for dramatic hydrogen production.

Acknowledgment

This work was supported by the New & Renewable Energy of the Korea Institute of Energy Technology Evaluation and Planning (KETEP) Grant funded by the Korea government Ministry of Knowledge Economy (no. 20103020050040).

References

[1] S. Xu, A. J. Du, J. Liu, J. Ng, and D. D. Sun, "Highly efficient CuO incorporated TiO_2 nanotube photocatalyst for hydrogen production from water," *International Journal of Hydrogen Energy*, vol. 36, no. 11, pp. 6560–6568, 2011.

[2] S. Xu, J. Ng, X. Zhang, H. Bai, and D. D. Sun, "Fabrication and comparison of highly efficient Cu incorporated TiO_2 photocatalyst for hydrogen generation from water," *International Journal of Hydrogen Energy*, vol. 35, no. 11, pp. 5254–5261, 2010.

[3] S. Onsuratoom, T. Puangpetch, and S. Chavadej, "Comparative investigation of hydrogen production over Ag-, Ni-, and Cu-loaded mesoporous-assembled TiO_2-ZrO_2 mixed oxide nanocrystal photocatalysts," *Chemical Engineering Journal*, vol. 173, no. 2, pp. 667–675, 2011.

[4] Q. Wang, N. An, Y. Bai et al., "High photocatalytic hydrogen production from methanol aqueous solution using the photocatalysts CuS/TiO_2 ," *International Journal of Hydrogen Energy*, vol. 38, no. 25, pp. 10739–10745, 2013.

[5] T. Miwa, S. Kaneco, H. Katsumata et al., "Photocatalytic hydrogen production from aqueous methanol solution with CuO/Al_2O_3/TiO_2 nanocomposite," *International Journal of Hydrogen Energy*, vol. 35, no. 13, pp. 6554–6560, 2010.

[6] M. Zhong, J. Shi, W. Zhang, H. Han, and C. Li, "Charge recombination reduction in dye-sensitized solar cells by depositing ultrapure TiO_2 nanoparticles on "inert" $BaTiO_3$ films," *Materials Science and Engineering B*, vol. 176, no. 14, pp. 1115–1122, 2011.

[7] L. S. Yoong, F. K. Chong, and B. K. Dutta, "Development of copper-doped TiO_2 photocatalyst for hydrogen production under visible light," *Energy*, vol. 34, no. 10, pp. 1652–1661, 2009.

[8] A. H. Gordillo, F. Tzompantzi, and R. Gómez, "An efficient ZnS-UV photocatalysts generated in situ from $ZnS(en)_{0.5}$ hybrid

during the H_2 production in methanol-water solution," *International Journal of Hydrogen*, vol. 37, no. 22, pp. 17002–17008, 2012.

[9] P. Gomathisankar, K. Hachisuka, H. Katsumata, T. Suzuki, K. Funasaka, and S. Kaneco, "Photocatalytic hydrogen production with CuS/ZnO from aqueous $Na_2S + Na_2SO_3$ solution," *International Journal of Hydrogen Energy*, vol. 38, no. 21, pp. 8625–8630, 2013.

[10] L. Qi, J. Yu, and M. Jaroniec, "Preparation and enhanced visible-light photocatalytic H_2-production activity of CdS-sensitized Pt/TiO_2 nanosheets with exposed (001) facets," *Physical Chemistry Chemical Physics*, vol. 13, no. 19, pp. 8915–8923, 2011.

[11] G. Lee and M. Kang, "Physicochemical properties of core/shell structured pyrite FeS_2/anatase TiO_2 composites and their photocatalytic hydrogen production performances," *Current Applied Physics*, vol. 13, no. 7, pp. 1482–1489, 2013.

[12] J. Kim and M. Kang, "High photocatalytic hydrogen production over the band gap-tuned urchin-like Bi_2S_3-loaded TiO_2 composites system," *International Journal of Hydrogen Energy*, vol. 37, no. 10, pp. 8249–8256, 2012.

[13] J. Kim, Y. Sohn, and M. Kang, "New fan blade-like core-shell $Sb_2Ti_xS_y$ photocatalytic nanorod for hydrogen production from methanol/water photolysis," *International Journal of Hydrogen Energy*, vol. 38, no. 10, pp. 2136–2143, 2013.

[14] P. Gao, J. Liu, T. Zhang, D. D. Sun, and W. Ng, "Hierarchical TiO_2/CdS "spindle-like" composite with high photodegradation and antibacterial capability under visible light irradiation," *Journal of Hazardous Materials*, vol. 229-230, pp. 209–216, 2012.

[15] H. Lee, Y. Park, and M. Kang, "Synthesis of characterization of Zn_xTi_yS and its photocatalytic activity for hydrogen production from methanol/water photo-splitting," *Journal of Industrial and Engineering Chemistry*, vol. 19, no. 4, pp. 1162–1168, 2013.

[16] C. Xing, Y. Zhang, W. Yan, and L. Guo, "Band structure-controlled solid solution of $Cd_{1-x}Zn_xS$ photocatalyst for hydrogen production by water splitting," *International Journal of Hydrogen Energy*, vol. 31, no. 14, pp. 2018–2024, 2006.

[17] T. T. ThanhThuy, P. Sheng, C. Huang et al., "Synthesis and photocatalytic application of ternary Cu-Zn-S nanoparticle-sensitized TiO_2 nanotube arrays," *Chemical Engineering Journal*, vol. 210, pp. 425–431, 2012.

[18] K. W. Cheng and C. J. Liang, "Preparation of Zn-In-S film electrodes using chemical bath deposition for photoelectrochemical applications," *Solar Energy Materials and Solar Cells*, vol. 94, no. 6, pp. 1137–1145, 2010.

[19] S. Sahai, M. Husain, V. Shanker, N. Singh, and D. Haranath, "Facile synthesis and step by step enhancement of blue photoluminescence from Ag-doped ZnS quantum dots," *Journal of Colloid and Interface Science*, vol. 357, no. 2, pp. 379–383, 2011.

[20] F. Jia, Z. Yao, and Z. Jiang, "Solvothermal synthesis ZnS-In_2S_3-Ag_2S solid solution coupled with $TiO_{2-x}S_x$ nanotubes film for photocatalytic hydrogen production," *International Journal of Hydrogen Energy*, vol. 37, no. 4, pp. 3048–3055, 2012.

[21] J. U. Kim, Y. K. Kim, and H. Yang, "Reverse micelle-derived Cu-doped $Zn_{1-x}Cd_xS$ quantum dots and their core/shell structure," *Journal of Colloid and Interface Science*, vol. 341, no. 1, pp. 59–63, 2010.

[22] K. W. Cheng, C. M. Huang, Y. C. Yu, C. T. Li, C. K. Shu, and W. L. Liu, "Photoelectrochemical performance of Cu-doped $ZnIn_2S_4$ electrodes created using chemical bath deposition," *Solar Energy Materials and Solar Cells*, vol. 95, no. 7, pp. 1940–1948, 2011.

[23] J. Sun, G. Chen, G. Xiong, J. Pei, and H. Dong, "Hierarchical microarchitectures of $AgGa_{1-x}In_xS_2$: long chain alcohol assisted synthesis, band gap tailoring and photocatalytic activities of hydrogen generation," *International Journal of Hydrogen Energy*, vol. 38, no. 25, pp. 10731–10738, 2013.

[24] H. Qi, J. Huang, L. Cao, J. Wu, and J. Li, "Controlled synthesis and optical properties of doughnut-aggregated hollow sphere-like CuS," *Ceramics International*, vol. 38, no. 8, pp. 6659–6664, 2012.

[25] J. Zhang, J. Yu, Y. Zhang, Q. Li, and J. R. Gong, "Visible light photocatalytic H_2-production activity of CuS/ZnS porous nanosheets based on photoinduced interfacial charge transfer," *Nano Letters*, vol. 11, no. 11, pp. 4774–4779, 2011.

[26] J. Yu and J. Ran, "Facile preparation and enhanced photocatalytic H_2-production activity of $Cu(OH)_2$ cluster modified TiO_2," *Energy and Environmental Science*, vol. 4, no. 4, pp. 1364–1371, 2011.

[27] J. Zhang, Z. Liu, B. Han et al., "Preparation of silica and TiO_2-SiO_2 core-shell nanoparticles in water-in-oil microemulsion using compressed CO_2 as reactant and antisolvent," *Journal of Supercritical Fluids*, vol. 36, no. 3, pp. 194–201, 2006.

[28] J. Du, G. Zhao, H. Pang, Y. Qian, H. Liu, and D. J. Kang, "A template method for synthesis of porous Sn-doped TiO_2 monolith and its enhanced photocatalytic activity," *Materials Letters*, vol. 93, pp. 419–422, 2013.

[29] F. Deng, Y. Li, X. Luo, L. Yang, and X. Tu, "Preparation of conductive polypyrrole/TiO_2 nanocomposite via surface molecular imprinting technique and its photocatalytic activity under simulated solar light irradiation," *Colloids and Surfaces A*, vol. 395, pp. 183–189, 2012.

[30] F. Li, T. Kong, W. Bi, D. Li, Z. Li, and X. Huang, "Synthesis and optical properties of CuS nanoplate-based architectures by a solvothermal method," *Applied Surface Science*, vol. 255, no. 12, pp. 6285–6289, 2009.

[31] G. P. Joshi, N. S. Saxena, R. Mangal, A. Mishra, and T. P. Sharma, "Band gap determination of Ni-Zn ferrites," *Bulletin of Materials Science*, vol. 26, no. 4, pp. 387–389, 2003.

[32] Y. Kim, J. H. Jeong, and M. Kang, "Rapid synthesis of bis (2,2′-bipyridine) nitratocopper(II) nitrate using a hydrothermal method and its application to dye-sensitized solar cells," *Inorganica Chimica Acta*, vol. 365, no. 1, pp. 400–407, 2011.

[33] S. Giraud, G. Loupias, H. Maskrot et al., "Dip-coating on TiO_2 foams using a suspension of Pt-TiO_2 nanopowder synthesized by laser pyrolysis-preliminary evaluation of the catalytic performances of the resulting composites in deVOC reactions," *Journal of the European Ceramic Society*, vol. 27, no. 2-3, pp. 931–936, 2007.

[34] J. Zhang, J. Yu, M. Jaroniec, and J. R. Gong, "Noble metal-free reduced graphene oxide-$ZnxCd_{1-x}S$ nanocomposite with enhanced solar photocatalytic H_2 production performance," *Nano Letters*, vol. 12, pp. 4584–4589, 2012.